Electronic Journal of Biotechnology 79 (2026) 100696

Contents lists available at ScienceDirect

Electronic Journal of Biotechnology

journal homepage: www.elsevier.com/locate/ejbt

Research article

ANKRD1 knockdown attenuates doxorubicin-induced dilated cardiomyopathy by regulating mitochondrial dysfunction and oxidative stress through activation of the AMPK/AKT/mTOR pathway ☆

Jia Yuan [a,1], Yu Zhou [b,1], GuoHua Wei [b], Tao Qi [b], HaoLiang Sun [c,*], Jian Shen [b,*]

[a] Department of Anesthesiology, The Affiliated Hospital of Xuzhou Medical University, Xuzhou City, Jiangsu Province, China
[b] Department of Anesthesiology, Jiangsu Province Hospital (The First Affiliated Hospital with Nanjing Medical University), Nanjing City, Jiangsu Province, China
[c] Department of Cardiovascular Surgery, Jiangsu Province Hospital (The First Affiliated Hospital with Nanjing Medical University), Nanjing City, Jiangsu Province, China

GRAPHICAL ABSTRACT

ANKRD1 knockdown attenuates doxorubicin-induced dilated cardiomyopathy by regulating mitochondrial dysfunction and oxidative stress through activation of the AMPK/AKT/mTOR pathway.

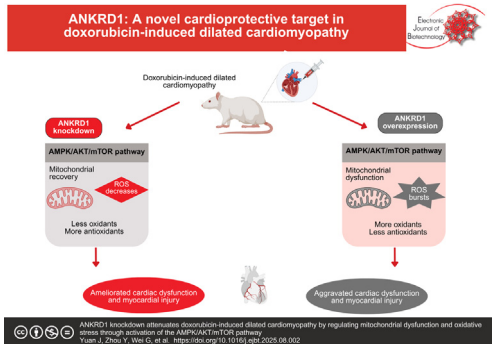

ARTICLE INFO

Article history:
Received 14 May 2025
Accepted 11 August 2025
Available online 11 November 2025

Keywords:
AMPK/AKT/mTOR pathway
ANKRD1
Ankyrin Repeat Domain 1 protein
Attenuates
Cardiomyocytes
Cardiomyopathy
Cardiovascular pathophysiology
Dilated cardiomyopathy

ABSTRACT

Background: Doxorubicin (DOX), a widely used chemotherapeutic agent, causes severe cardiotoxicity that frequently progresses to dilated cardiomyopathy (DCM). While ankyrin repeat domain 1 protein (ANKRD1) plays critical roles in cardiovascular pathophysiology, its specific involvement in doxorubicin-induced DCM remains unknown. This study investigates the functional significance of ANKRD1 in DOX-induced DCM pathogenesis.
Results: DOX treatment significantly upregulated ANKRD1 expression in both rat models and H9c2 rat cardiomyocytes. *In vivo*, ANKRD1 knockdown ameliorated DOX-induced cardiac dysfunction, as demonstrated by improved left ventricular ejection fraction and fractional shortening, along with reduced serum levels of lactate dehydrogenase and creatine kinase-myocardial band. Conversely, ANKRD1 overexpression exacerbated cardiac impairment. Pathological examination revealed that ANKRD1 knockdown attenuated DOX-induced myocardial tissue damage and collagen deposition, while ANKRD1 overexpression intensified these pathological changes. Furthermore, ANKRD1 knockdown mitigated mitochondrial dysfunction and oxidative stress in DCM models both *in vivo* and *in vitro*. Mechanistically, ANKRD1

☆ Audio abstract available in Supplementary material.
Peer review under responsibility of Pontificia Universidad Católica de Valparaíso.
* Corresponding authors.
E-mail addresses: shlshl_in_jsph@hotmail.com (H. Sun), sjshenjian_jsph@outlook.com (J. Shen).
[1] These authors contributed equally to this work.

https://doi.org/10.1016/j.ejbt.2025.08.002

Doxorubicin
Mitochondrial damage
Oxidative stress

knockdown activated the AMP-activated protein kinase (AMPK)/protein kinase B (AKT)/mammalian target of rapamycin (mTOR) signaling cascade, thereby attenuating DOX-induced cardiomyocyte toxicity, mitochondrial dysfunction, and oxidative stress. Rescue experiments using the AMPK inhibitor dorsomorphin confirmed this pathway's involvement, as dorsomorphin treatment abolished the protective effects of ANKRD1 knockdown against DOX-induced cardiomyocyte damage.
Conclusions: ANKRD1 knockdown prevents DOX-induced DCM by ameliorating mitochondrial dysfunction and oxidative stress through activation of the AMPK/AKT/mTOR pathway. These findings establish ANKRD1 as a promising therapeutic target for preventing DOX-induced cardiotoxicity and DCM.
How to cite: Yuan J, Zhou Y, Wei G, et al. ANKRD1 knockdown attenuates doxorubicin-induced dilated cardiomyopathy by regulating mitochondrial dysfunction and oxidative stress through activation of the AMPK/AKT/mTOR pathway. Electron J Biotechnol 2026, 79. https://doi.org/10.1016/j.ejbt.2025.08.002.

1. Introduction

Dilated cardiomyopathy (DCM) usually refers to left ventricular enlargement and myocardial contractile dysfunction in the absence of abnormal load or severe coronary artery disease sufficient to account for cardiac dysfunction [1,2]. DCM may result from various causes, including genetic mutations, infections, inflammation, autoimmunity, toxins, and endocrine or neuromuscular disorders [3,4]. Currently, different treatment strategies are used clinically according to the etiology, clinical symptoms, and severity of DCM, and the treatment as a whole focuses mainly on controlling symptoms, reducing the risk of sudden cardiac death, and improving the structural and electrical complications of disease progression. Since DCM patients often experience a gradual onset with an unknown etiology, they are typically diagnosed when heart failure is already advanced, leading to a poor prognosis and a 10-year mortality rate of around 40% [5]. Therefore, new diagnostic methods and therapeutic strategies for DCM still need to be further explored.

As a member of the anthraquinone class, Doxorubicin (DOX) is extensively utilized as a first-choice antitumor drug for managing different malignant solid tumors and acute lymphomas. However, despite significantly improving long-term survival in cancer patients, DOX's clinical utility is limited by cumulative dose-dependent cardiotoxicity that frequently progresses to DCM [6,7]. Although the mechanism by which DOX induces DCM has not been fully elucidated, mitochondrial dysfunction and oxidative stress are thought to be involved [8]. The heart, as a constant biological pump that requires a constant supply of energy, consumes the most energy [9]. Energy is primarily produced in the mitochondria, with adenosine triphosphate (ATP) being generated through the electron transport chain and oxidative phosphorylation (OXPHOS) systems to maintain normal myocardial physiological function [10,11]. Mitochondrial dysfunction significantly contributes to DCM development and could be a key focus for targeting DOX-induced DCM [12,13,14,15]. OXPHOS is a major source of mitochondrial ATP and a major site of reactive oxygen species (ROS) production. Cardiac ROS signaling under physiological conditions regulates cardiomyocyte maturation, cardiac calcium, excitation–contraction coupling, and vascular tone. Pathological disturbances in ROS regulation can trigger ROS overaccumulation, resulting in oxidative stress, a major contributor to DCM pathogenesis [16,17]. Experimental evidence demonstrates that DOX induces oxidative damage in cardiac cells, characterized by elevated malondialdehyde (MDA) levels and suppressed superoxide dismutase (SOD) activity in primary cardiomyocytes. These findings are corroborated by *in vivo* studies where DOX-treated rats exhibited significantly decreased cardiac SOD activity and increased MDA content compared to controls, driving substantial lipid peroxidation product accumulation and severe oxidative stress [18,19]. Previous research consistently highlights the pivotal role of oxidative stress in DOX-induced DCM pathogenesis [20,21]. Consequently, targeted modulation of mitochondrial dysfunction and oxidative stress at myocardial lesion sites represents a promising precision therapeutic strategy for DCM management.

Ankyrin repeat domain 1 protein (ANKRD1), known for its high conservation and multifunctionality, is thought to play a part in cardiogenesis, mechanoreception, gene expression regulation, intracellular signaling, and the cardiac stress response. ANKRD1 mutations are directly associated with DCM due to disruption of normal signaling in cardiac torsion [22]. As established in prior research, ANKRD1 expression is significantly upregulated in patients with DCM and ischemic cardiomyopathy [23]. Elevated ANKRD1 levels in idiopathic DCM correlate with reduced cardiac contractility and compliance, positioning this protein as a potential biomarker for cardiac remodeling and disease progression [24]. Transcriptomic analyses further identify ANKRD1 as a core differentially expressed gene distinguishing DCM from non-heart failure states, with expression patterns predictive of DCM diagnosis and inversely correlated with left ventricular ejection fraction (LVEF) [25]. Complementary murine models reveal that cardiomyocyte-specific ANKRD1 overexpression initially preserves ejection fraction and muscle fiber force akin to hypertrophic cardiomyopathy phenotypes, but ultimately progresses to myxomatous degeneration characteristic of DCM [26,27]. Furthermore, ANKRD1 deficiency blunts cardiac damage and remodeling in experimental autoimmune myocarditis models, preserving cardiac function during post-myocarditis DCM development [28].

Therefore, the present study mimicked DCM *in vitro* and *in vivo* by treating rats and H9c2 cells with DOX, and then investigated the effect of ANKRD1 on DOX-induced DCM and its potential mechanism by gain-or-loss-of-function experiments.

2. Materials and methods

2.1. Animals and experimental protocol

Sprague-Dawley rats, aged 8 weeks and weighing between 220 and 260 g, were acquired from Beijing Vital River Laboratory Animal Technology Co., Ltd. (Beijing, China). They were kept in a specific pathogen-free setting with a temperature range of 21–25°C, a 12 h light/dark cycle, and unlimited access to food and water. To minimize the potential impact of environmental factors on experimental outcomes, the rats were acclimated for one week prior to the initiation of the experiment. This experiment was approved and reviewed by Jiangsu Province Hospital Animal Ethics Committee (No. 2021-SRFA-023).

Rats were randomly allocated using a random number table into two groups (n = 20 per group): vehicle control (Control) and DOX-treated (DCM). The DCM model was established following previously published protocols [29,30,31,32], with minor adjustments based on our preliminary experiments. DOX (Solarbio, Beijing, China) was dissolved in 0.9% saline and administered via intraperitoneal injection at a dose of 2.5 mg/kg body weight every five days for six cycles (on days 0, 6, 12, 18, 24, and 30), yielding a cumulative dose of 15 mg/kg. Control rats received an equivalent volume of 0.9% saline at the same timepoints.

To investigate ANKRD1's role *in vivo*, a separate cohort was randomized into four groups (n = 20 per group): ANKRD1 overexpression (AAV9-ANKRD1 + DOX), ANKRD1 knockdown (AAV9-shANKRD1 + DOX), overexpression control (AAV9-NC + DOX), and knockdown control (AAV9-shNC + DOX). Cardiac-specific modulation was achieved through intramyocardial injection of adeno-associated virus (AAV) 9 vectors (2×10^{11} vector genomes/rat, Hanbio Biotechnology, Shanghai) expressing ANKRD1 or shRNA under the cardiac troponin T promoter. Four weeks post-AAV9 administration, DOX treatment commenced to induce DCM.

The DCM model was successfully induced in 85% of the animals, based on echocardiographic criteria, which defined DCM as LVEF < 60% and left ventricular fractional shortening (LVFS) < 25%. Throughout the experimental period, eighteen rats died prior to the scheduled endpoint, distributed as follows: DOX-only (n = 3), AAV9-NC + DOX (n = 3), AAV9-shNC + DOX (n = 4), AAV9-ANKRD1 + DOX (n = 5), and AAV9-shANKRD1 + DOX (n = 3). Mortality peaked during weeks 4–6 of DOX treatment, with necropsy-confirmed causes of acute heart failure or sudden cardiac death consistent with established model progression [29]. No mortality occurred in vehicle controls. Two additional animals were excluded pre-analysis for non-protocol reasons: one developed severe pneumonia (day 18) and another succumbed to a procedural complication during injection (day 12). These exclusions followed predefined DOX-independent criteria to preserve analytical integrity. We confirm these attrition events were incorporated into statistical power calculations and did not affect the validity of intergroup comparisons or final outcomes.

One week after the DOX injection, 1% pentobarbital sodium (50 mg/kg) anesthetized rats were subjected to transthoracic echocardiography to assess cardiac function. Blood samples were collected before euthanasia, and myocardial tissue samples were collected and stored at −80°C. To ensure experimental reproducibility, a minimum of five biological replicates per group were analyzed in subsequent *in vivo* experiments.

2.2. Measurement of cardiac function

Echocardiography was performed on anesthetized rats using a transthoracic echocardiography system (VisualSonics, Canada). LVEF and LVFS were calculated from three consecutive cardiac cycles.

2.3. Enzyme-linked immunosorbent assay (ELISA)

Rat right common carotid artery blood (4 mL) was centrifuged at 3000 r/min at 4°C for 10 min. The resulting serum was detected using ELISA kits for creatine kinase-myocardial band (CK-MB) and Lactate dehydrogenase (LDH) (MLBIO, Shanghai, China).

2.4. Histological examination

Rat cardiac tissues were fixed overnight in 4% paraformaldehyde, dehydrated with a series of alcohol concentrations, permeabilized using xylene, and embedded in paraffin to produce 5 μm thick slices. The sections of the specimens were evaluated under a light microscope (Olympus, Tokyo, Japan) after being stained with hematoxylin-eosin (HE), Masson's trichrome, and were then observed for morphological changes and fibrosis in the myocardium.

For HE staining, slices were routinely dewaxed and successively treated with hematoxylin and eosin for 10 min, 1% hydrochloric acid for 10 s, 2% sodium bicarbonate for 10 s, and eosin staining solution for 3 min. Following gradient alcohol dehydration and xylene permeabilization, slices were sealed with neutral resin and observed under a light microscope.

For Masson's trichrome staining, Masson's Trichrome Stain Kit (Solarbio) was used. Weigert's iron hematoxylin staining solution was prepared prior to use. Tissue sections were routinely dewaxed and stained with Weigert's iron hematoxylin staining solution for 10 min. Excess stain was removed by rinsing with distilled water. Acid differentiation solution was then applied for 12 s, followed by another 30 s distilled water rinse. Sections were blued by applying Masson bluing solution for 3–5 min and rinsed again with distilled water for 30 s. Ponceau-fuchsin was applied for 8 min. A weak acid working solution was prepared by mixing distilled water with the weak acid solution in a 2:1 ratio and applied for 30 s after the ponceau-fuchsin staining step. After tipping off excess liquid, phosphomolybdic acid solution was applied for 1–2 min, followed by a 30-s rinse with the weak acid working solution. Excess liquid was removed before applying aniline blue staining solution for 1 min, concluding with a final 30 s rinse using the weak acid working solution. Following gradient alcohol dehydration and xylene permeabilization, slices were sealed with neutral resin and observed under a light microscope. The percentage of fibrosis was calculated by using ImageJ software.

2.5. Detection of mitochondrial ROS

Mitochondrial ROS were detected in myocardial frozen sections using the MitoSOX™ Green (M36005, Thermo Fisher Scientific, Waltham, MA, USA) based on the manufacturers' instructions. Briefly, frozen sections were incubated with 5 μM MitoSOX at 37°C for 30 min protected from light and then washed with phosphate-buffered saline (PBS). The intensity of green fluorescence was observed under a fluorescence microscope (Leica, Wetzlar, Germany).

2.6. Immunohistochemistry

Myocardial tissue paraffin sections were deparaffinized, placed in citrate antigen repair buffer, incubated with 3% hydrogen peroxide solution for 25 min, blocked with 3% BSA for 30 min, and incubated with primary antibody 4-hydroxynonenal (4-HNE; 1:200, ab48506, Abcam, Cambridge, USA) at 4°C overnight and secondary antibody (Abcam) at room temperature for 50 min. DAB color solution was dropped, followed by hematoxylin counterstaining. After dehydration and sealing, photographs were taken under a light microscope (Olympus).

2.7. Cell culture and experimental protocol

The H9c2 rat cardiomyocyte line (CRL-1446, ATCC, Manassas, VA) was maintained in Dulbecco's Modified Eagle Medium (DMEM; Thermo Fisher Scientific) supplemented with 10% fetal bovine serum, 100 U/mL penicillin, and 100 μg/mL streptomycin at 37°C in a humidified 5% CO_2 atmosphere.

To establish the injury model, H9c2 cells at 80% confluence were exposed to 1 μM doxorubicin (DOX) for 24 h, while control cells received equal volumes of phosphate-buffered saline.

For *in vitro* investigation of ANKRD1′s role, H9c2 cells were plated in 6-well plates for 24 h and then transfected with ANKRD1 overexpression lentivirus (oeANKRD1) or knockdown lentivirus (shANKRD1) and their corresponding negative controls (oeNC or shNC), constructed by Genechem (Shanghai, China), respectively. After 12 h post-transfection, cells were cultured in complete medium for 72 h. Stable transductants were selected using 2 μg/mL puromycin-containing medium. Successful ANKRD1 modulation was confirmed by Western blotting prior to subsequent 24-h treatment with 0.5 μM DOX.

For pathway validation, lentivirus-transduced H9c2 cells were pretreated with 10 μM AMP-activated protein kinase (AMPK) inhibitor dorsomorphin (HY-13418A; MedChemExpress, USA) for 30 min before 24 h exposure to 1 μM DOX.

2.8. Cell Counting Kit-8 (CCK-8) assay

Cell viability was measured using the CCK-8 kit (Solarbio) according to the manufacturer's instructions. After indicated treatments, cells were seeded at 2×10^4 cells/well in 96-well plates and incubated overnight, followed by the addition of 10 μL CCK-8 solution to 100 μL DMEM for 2 h. Absorbance was measured at 450 nm using a fully automated microplate reader (Bio-Rad, USA).

2.9. LDH assay

LDH release into culture supernatants served as a cytotoxicity indicator. Following specified treatments, supernatants were collected and LDH levels quantified using an LDH Release Assay Kit (C0019S, Beyotime, Shanghai, China) per manufacturer's protocol. Absorbance measurements were obtained at 490 nm using a Bio-Rad microplate reader.

2.10. Mitochondrial membrane potential (MMP) assay

Prepare the JC-1 staining working solution following the manufacturer's instructions (C2003S, Beyotime). Harvest 3×10^5 cells and resuspend in 0.5 mL culture medium. Add 0.5 mL freshly prepared JC-1 working solution, mixing thoroughly by inverting the tube several times. Incubate cells at 37°C for 20 min in a culture incubator. After incubation, centrifuge at 600 g for 3–4 min at 4°C to pellet cells. Discard the supernatant and perform two washing cycles: First, resuspend the pellet in 1 mL JC-1 staining buffer and centrifuge at 600 g (4°C, 3–4 min). Discard supernatant, then repeat this wash procedure once more. Finally, resuspend cells in an appropriate volume of JC-1 staining buffer. MMP analysis was conducted using a BD FACSCanto II flow cytometer (Becton Dickinson, NY, USA), with fluorescence data (red/green ratio) processed through FlowJo software.

2.11. Detection of intracellular and mitochondrial ROS

As instructed by the manufacturer, cells were incubated with 10 μM 2, 7-dichlorodihydrofluorescein diacetate (DCFH-DA, S0033M, Beyotime) at 37°C for 20 min or 5 μM MitoSOX (M36005, Thermo Fisher Scientific) at 37°C for 10 min and detected on a flow cytometer (Becton Dickinson). Fluorescence data were processed with FlowJo software.

2.12. ATP Measurement

ATP levels in cells and tissues were quantified using a commercial ATP assay kit (S0027, Beyotime). Supernatants from rat myocardial lysates and cellular preparations were collected and processed with the ATP-detection lysis buffer provided in the kit. An appropriate volume of ATP detection working solution was freshly prepared at a ratio of 100 μL per sample or standard. This working solution was then transferred to all cellular and tissue samples. Relative light units were measured using a luminometer, with ATP concentrations subsequently determined from the standard calibration curve according to the manufacturer's instructions.

2.13. Measurement of MDA, SOD and glutathione (GSH)

MDA content, SOD activity, and GSH levels were quantified in rat myocardial tissue homogenates and cellular supernatants using standardized commercial assays. MDA was measured via thiobarbituric acid reaction, SOD activity determined by xanthine oxidase method, and GSH content assessed colorimetrically, employing corresponding detection kits (A003-1-2 for MDA, A001-1-2 for SOD, A005-1-2 for GSH; Nanjing Jiancheng Bioengineering Institute, Jiangsu, China) strictly according to the manufacturer's protocols.

2.14. Western blot

Total protein was extracted from myocardial tissue homogenates and cells using Radio-immunoprecipitation assay buffer (Beyotime), followed by quantification by BCA kit (Beyotime). Then, 20 μg protein was separated by SDS-PAGE (Beyotime), transferred to PVDF membranes (Millipore, USA), blocked with 50 g/L skimmed milk powder-TBST solution for 1 h, and combined with primary antibodies including ANKRD1 (1:1000, #A6192, Abclonal, Wuhan, China), AMPK (1:1000, #5832, CST, MA, USA), phosphorylated AMPK (p-AMPK; 1:1000, #50081, CST), protein kinase B(AKT; 1:1000, #4691T, CST), phosphorylated AKT (p-AKT; 1:1000, #4060T, CST), mammalian target of rapamycin (mTOR; 1:1000, #2983, CST), phosphorylated mTOR (p-mTOR; 1:1000, #5536, CST), and β-actin (1:5000, 81115-1-RR, Proteintech). Horseradish peroxidase-labeled corresponding secondary antibody (1:5000, CST) was allowed to incubate for 1 h. Color development was facilitated using ECL (Pierce, CA, USA) in the ChemiDoc™ MP system (Bio-Rad). Quantification was analyzed by ImageJ software.

2.15. Reverse transcription-quantitative polymerase chain reaction (RT-qPCR)

Total RNA was extracted by TRIzol reagent (Invitrogen), and the concentration and purity of RNA were detected by UV spectrophotometer (Thermo Fisher Scientific). mRNA cDNA was synthesized using PrimeScript™ RT reagent kit (TAKARA, Shiga, Japan) and detected using SYBR Green Master Mix (Thermo Fisher Scientific) on the Applied Biosystems 7500 Fast Real-Time PCR system (Applied Biosystems, CA, USA). The samples were pre-denatured by heating at 95°C for 30 s, followed by 40 cycles of amplification (5 s at 95°C and 34 s at 60°C) and finally dissociation (15 s at 95°C, 1 min at 60°C, and 15 s at 95°C). Gene calculation was done with the $2^{-\Delta\Delta Ct}$ method using β-actin as an internal reference. Designed PCR primers (Sangong, Shanghai, China) are found in Table 1.

Genomic DNA was extracted from cardiac tissues and H9C2 cardiomyocytes using a DNA extraction kit (Tiangen, Beijing, China). To detect mitochondrial DNA (mtDNA) copy numbers, DNA was analyzed using RT-qPCR with primers specific to mtDNA. (Table 1).

2.16. Statistical analysis

Data were statistically analyzed using GraphPad Prism (version 10.0), and presented as mean ± standard deviation. Two groups were compared using a *t*-test, and multiple groups were evaluated

Table 1
Primers.

	Sequences (5′ – 3′)
mtDNA	Forward: GCCTATCGAGCTTGGTGATA Reverse: TATCCTACCTTTGCACGGTC
nDNA	Forward: CAAGGCCAAGTCCACAAGTC Reverse: ACAAAGCGCAGGAAGAAGTG
ANKRD1	Forward: GTTCCTTCCTGGCGAGTTCA Reverse: TTCCGTTGTTCTTCCCCCAG
β-actin	Forward: TGCTATGTTGCCCTAGACTTCG Reverse: GTTGGCATAGAGGTCTTTACGG

Note: mtDNA, mitochondrial DNA; nDNA, nuclear DNA; ANKRD1, ankyrin repeat domain 1.

with one-way or two-way ANOVA, followed by Tukey's post hoc test. Statistical significance was determined at $p < 0.05$ ($^{*}p < 0.05$, $^{**}p < 0.01$, $^{***}p < 0.001$; ns, not significant).

3. Results

3.1. DOX induces upregulation of ANKRD1

Successful establishment of the DOX-induced DCM model (Fig. 1A) was confirmed through multimodal validation. Echocardiography revealed significant impairment of cardiac function in DOX-treated rats, evidenced by reduced LVEF (40.79 ± 4.14% vs 61.7 ± 4.52% in controls; $p < 0.001$) and fractional shortening (LVFS: 16.59 ± 3.57% vs 34.32 ± 4.43%; $p < 0.001$) (Fig. 1B; *t*-test). Serum biomarkers confirmed myocardial injury, with elevated CK-MB and LDH levels (both $p < 0.001$, Fig. 1C; *t*-test). Histopathological examination demonstrated characteristic DCM alterations: HE staining showed interstitial edema, nuclear deformation, and structural disorganization in myocardial tissue (Fig. 1D), while Masson trichrome staining confirmed substantial collagen deposition (16.96 ± 2.03% vs 4.91 ± 1.19% in controls; $p < 0.001$) (Fig. 1E; *t*-test). These findings collectively validated the DCM model. Parallel *in vitro* experiments using H9c2 cardiomyocytes exposed to 1 μM DOX for 24 h recapitulated key injury phenotypes: Cell viability decreased to approximately 57.0% of the Control group ($p < 0.01$, Fig. 1F; *t*-test), accompanied by increased LDH release ($p < 0.001$, Fig. 1G; *t*-test).

Next, we examined ANKRD1 in the DCM model. ANKRD1 expression was significantly upregulated at both transcriptional (approximately 3.2-fold increase; $p < 0.001$) and translational levels (approximately 5-fold increase; $p < 0.001$) following DOX administration (Fig. 2A, B; *t*-test). Consistent with *in vivo* findings, DOX exposure elevated ANKRD1 expression in H9c2 cells (mRNA: 2.86-fold, $p < 0.001$, *t*-test; protein: 1.59-fold, $p < 0.001$) (Fig. 2C, D; *t*-test).

3.2. ANKRD1 knockdown attenuates DOX-induced cardiac dysfunction and myocardial tissue injury in rats

Cardiac-specific modulation of ANKRD1 expression was achieved through pre-DOX AAV9 administration, as confirmed by Western blot (all groups $p < 0.05$ vs. respective controls) (Fig. 3A; *t*-test). Functionally, ANKRD1 knockdown significantly improved cardiac parameters, elevating both LVEF and LVFS ($p < 0.001$ vs. AAV9-shNC + DOX group), while ANKRD1 overexpression exacerbated cardiac dysfunction (LVEF: $p < 0.05$; LVFS: $p < 0.01$ vs. AAV9-NC + DOX group) (Fig. 3B; one-way ANOVA with Tukey's post hoc test). Biochemically, ANKRD1 knockdown attenuated DOX-induced elevations in serum CK-MB and LDH ($p < 0.001$), whereas ANKRD1 overexpression further increased these biomarkers (CK-MB: $p < 0.05$; LDH: $p < 0.001$) (Fig. 3C; one-way ANOVA with Tukey's post hoc test). Histopathological analysis demonstrated that ANKRD1 knockdown mitigated DOX-induced myocardial tissue injury and collagen deposition, while ANKRD1 overexpression potentiated these pathological changes (Fig. 3D, E).

3.3. ANKRD1 knockdown alleviates DOX-induced mitochondrial dysfunction and oxidative stress in rats

DOX treatment significantly reduced myocardial mtDNA copy number (55% decrease, $p < 0.001$) and ATP content (49% decrease, $p < 0.001$). ANKRD1 knockdown reversed these deficits (both $p < 0.001$ vs. AAV9-shNC + DOX), whereas ANKRD1 overexpression exacerbated mitochondrial impairment (mtDNA: $p < 0.01$; ATP: $p < 0.05$ vs. AAV9-NC + DOX) (Fig. 4A–B; one-way ANOVA with Tukey's post hoc test).

Further, DOX treatment significantly elevated MDA levels while suppressing SOD activity and GSH content (all $p < 0.001$ vs. Control). ANKRD1 knockdown attenuated these oxidative perturbations, reducing MDA ($p < 0.001$) and restoring GSH ($p < 0.05$) versus AAV9-shNC + DOX group. Conversely, ANKRD1 overexpression exacerbated DOX-induced oxidative damage, further elevating MDA ($p < 0.001$) and suppressing antioxidant activities ($p < 0.05$) (Fig. 4C; one-way ANOVA with Tukey's post hoc test). Mitochondrial ROS assessment revealed parallel effects: DOX elevated ROS, which was normalized by ANKRD1 knockdown but amplified by ANKRD1 overexpression (Fig. 4D). The analysis of 4-HNE, a peroxidation product, in myocardial tissue through immunohistochemistry revealed (Fig. 4E) that DOX treatment elevated myocardial 4-HNE levels. This elevation was reduced by knocking down ANKRD1, but increased with its overexpression.

3.4. ANKRD1 knockdown attenuates DOX-induced cardiomyocyte injury, mitochondrial dysfunction, and oxidative stress

To further validate the protective role of ANKRD1 in DOX-induced cardiomyocyte injury, H9c2 cells were treated with lentiviruses knocking down or overexpressing ANKRD1, respectively, prior to DOX intervention. Western blot verified the alteration of ANKRD1 expression in the cells (all groups $p < 0.01$ vs. respective controls) (Fig. 5A; *t*-test). Silencing ANKRD1 reversed the reduction in cell viability ($p < 0.01$ vs. shNC + DOX) and the rise in LDH release ($p < 0.05$ vs. shNC + DOX) due to DOX, whereas overexpressing ANKRD1 intensified the myocardial cytotoxicity caused by DOX (cell viability: $p < 0.05$; LDH release: $p < 0.01$ vs. oeNC + DOX) (Fig. 5B, C; one-way ANOVA with Tukey's post hoc test). ANKRD1 knockdown significantly attenuated DOX-induced mitochondrial dysfunction in cardiomyocytes, which was mainly manifested as increased mtDNA copy number ($p < 0.01$), enhanced ATP synthesis ($p < 0.01$), and reduced MMP depolarization ($p < 0.001$). ANKRD1 overexpression further aggravated DOX-induced mitochondrial dysfunction in cardiomyocytes (mtDNA: $p < 0.05$; MMP: $p < 0.05$ vs. oeNC + DOX) (Fig. 5D–F; one-way ANOVA with Tukey's post hoc test). Flow cytometry assay revealed that ANKRD1 knockdown reversed the upregulation of mitochondrial ROS ($p < 0.05$ vs. shNC + DOX) and intracellular ROS ($p < 0.001$ vs. shNC + DOX) levels by DOX, and ANKRD1 overexpression had the opposite effect (mitochondrial ROS: $p < 0.05$; intracellular ROS: $P < 0.01$ vs. oeNC + DOX) (Fig. 5G, H; one-way ANOVA with Tukey's post hoc test). A significant increase in cellular MDA ($p < 0.01$) and a decrease in SOD ($p < 0.001$) and GSH ($p < 0.001$) were induced by DOX; however, knocking down ANKRD1 reduced MDA ($p < 0.05$) and enhanced SOD ($p < 0.05$) and GSH ($p < 0.01$) activities, whereas overexpressing ANKRD1 produced the opposite results, further elevating MDA ($p < 0.01$) and suppressing GSH ($p < 0.01$) (Fig. 5I; one-way ANOVA with Tukey's post hoc test).

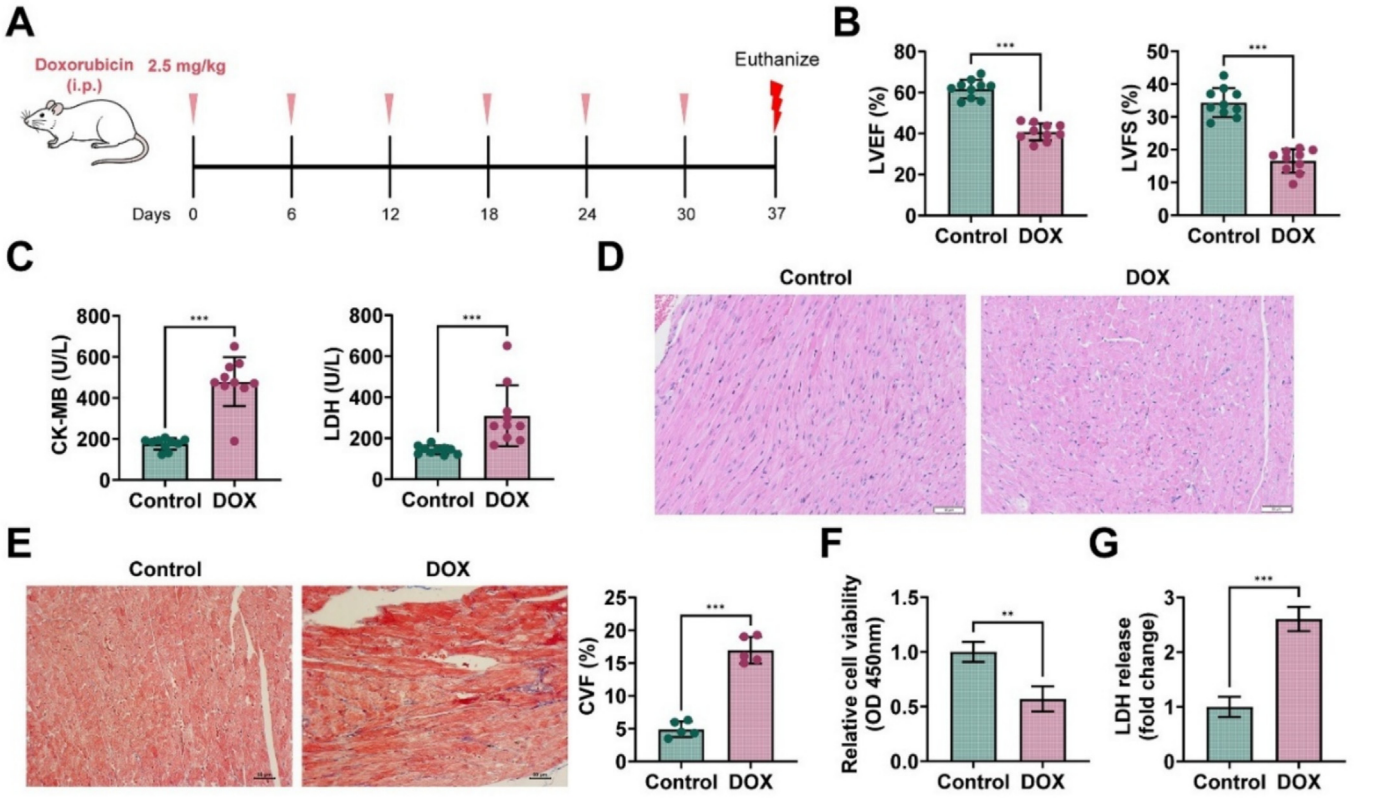

Fig. 1. Doxorubicin-induced model of cardiomyopathy. (A) Schematic diagram of dose schedule for DOX-induced DCM model; (B) Echocardiography to detect LVEF and LVFS in rats of each group (n = 10 rats per group); (C) Serum CK-MB and LDH levels in rats of each group (n = 10 rats per group); (D): Representative images of HE staining of myocardial tissues (n = 5 rats per group; scale bar: 50 μm); (E) Masson staining to assess collagen fiber area of myocardial tissues in rats of each group (n = 5 rats per group; scale bar: 50 μm); (F) CCK8 assay to detect cell viability (n = 3 biological replicates per group); (G) Kit to detect cellular LDH release level (n = 3 biological replicates per group). * $p < 0.05$, ** $p < 0.01$, *** $p < 0.001$, NS: not significant. All statistical analyses were performed by *t* test.

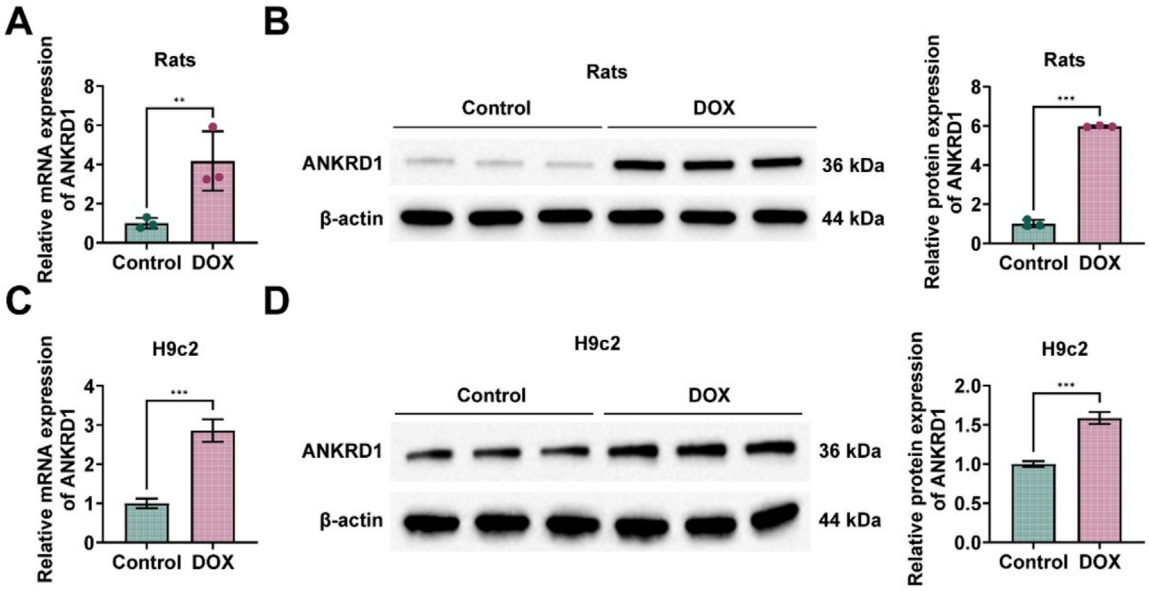

Fig. 2. DOX-induced upregulation of ANKRD1. (A-B): RT-qPCR and Western blot detection of ANKRD1 mRNA and protein expression levels in myocardial tissues in rats of each group (n = 3 rats per group); (C-D) RT-qPCR and Western blot to detect cellular ANKRD1 mRNA and protein expression level (n = 3 biological replicates per group). * $p < 0.05$, ** $p < 0.01$, *** $p < 0.001$, NS: not significant. All statistical analyses were performed by *t* test.

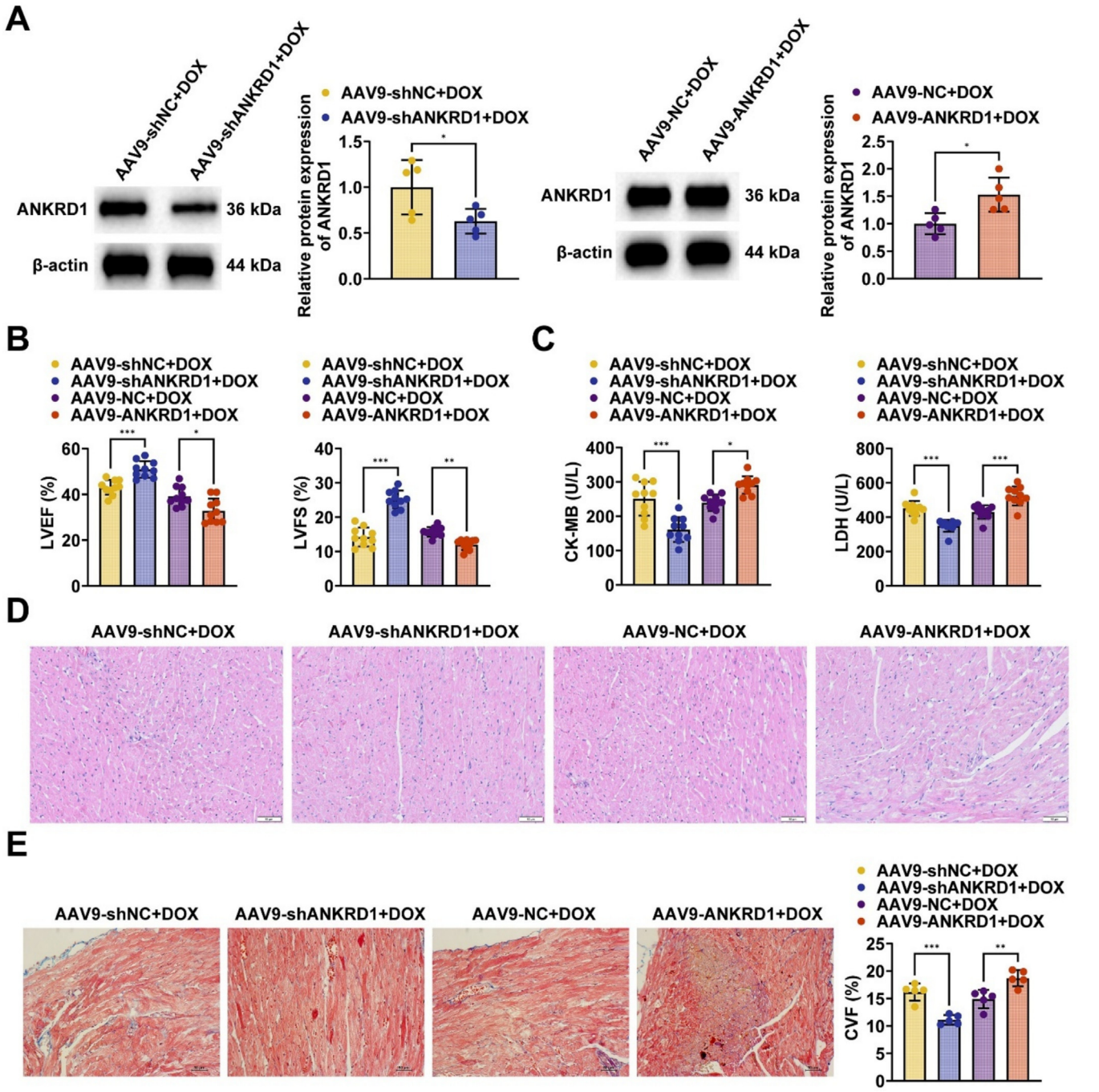

Fig. 3. ANKRD1 knockdown attenuates DOX-induced cardiac dysfunction and myocardial tissue damage in rats. (A) Western blot detection of protein expression level of ANKRD1 in rat myocardial tissues (n = 5 rats per group); (B) Echocardiography detection of LVEF and LVFS in rats of each group (n = 10 rats per group); (C) Determination of serum CK-MB and LDH levels in rats of each group (n = 10 rats per group); (D) Representative images of HE staining of myocardial tissues in rats of each group (n = 5 rats per group; scale bar: 50 μm); (E) Masson staining to assess the collagen fiber area of myocardial tissue in rats of each group (n = 5 rats per group; scale bar: 50 μm). * $p < 0.05$, ** $p < 0.01$, *** $p < 0.001$, NS: not significant. One-way ANOVA followed by Tukey's post hoc test was used in (B-E), *t* test was used in (A).

3.5. AMPK/AKT/mTOR pathway is involved in DCM and affected by ANKRD1

The process by which DOX injures cardiomyocytes is associated with the accumulation of ROS and an imbalance in energy metabolism, with mTOR molecules involved in regulating this process. As central mediators in protein interactions, mTOR-associated proteins play a pivotal role in connecting autophagy with oxidative stress signaling driven by energy metabolism [33]. Western blot detection found that in the myocardial tissues of DCM rats, p-AMPK levels decreased ($p < 0.001$) while p-AKT ($p < 0.05$) and p-mTOR ($p < 0.01$) levels increased; however, knocking down ANKRD1 reversed these protein expression trends (all $p < 0.001$ vs. AAV9-shNC + DOX group), whereas overexpressing ANKRD1 had the opposite impact (p-AMPK/AMPK: $p < 0.05$; p-AKT/AKT: $p < 0.01$; p-mTOR/mTOR: $p < 0.01$ vs. AAV9-NC + DOX group) (Fig. 6A; one-way ANOVA with Tukey's post hoc test). These findings suggest that ANKRD1 knockdown activates the AMPK/AKT/mTOR signaling cascade in myocardial tissues of DCM rats. *In vitro* experiments

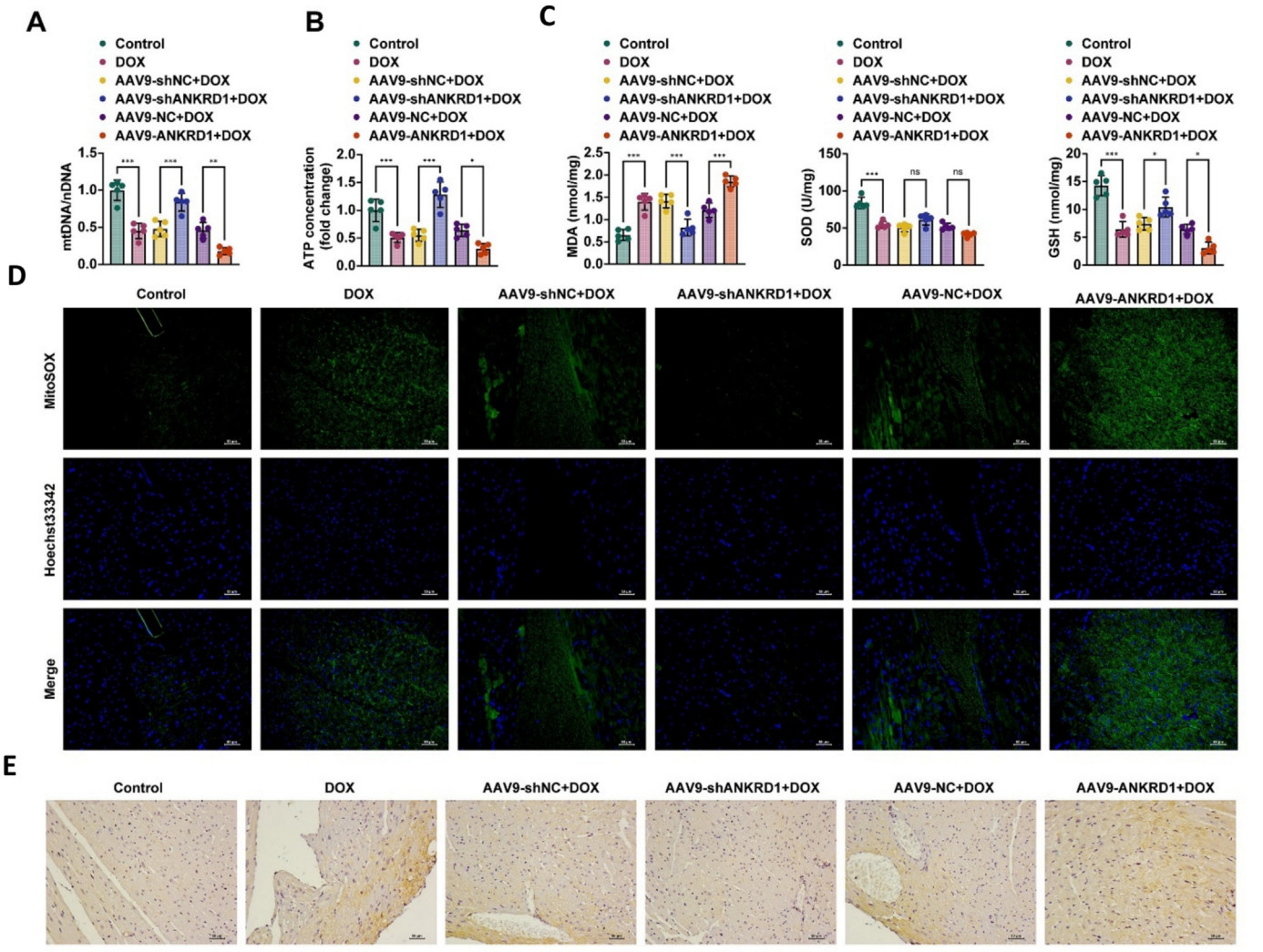

Fig. 4. ANKRD1 knockdown alleviates DOX-induced mitochondrial dysfunction and oxidative stress in rats. (A) RT-qPCR to detect mtDNA copy number in rat myocardial tissue (n = 5 rats per group); (B) Kit to detect ATP content in rat myocardial tissue (n = 5 rats per group); (C) Kits to detect MDA, SOD, and GSH levels (n = 5 rats per group); (D) MitoSOX staining to assess mitochondrial ROS level in rat myocardial tissue (n = 5 rats per group; scale bar: 50 μm); (E) Representative images of immunohistochemistry of rat myocardial tissue 4-HNE in each group (n = 5 rats per group; scale bar: 50 μm). * $p < 0.05$, ** $p < 0.01$, *** $p < 0.001$, NS: not significant. All statistical analyses were performed by one-way ANOVA followed by Tukey's post hoc test.

further validated
these findings (Fig. 6B; one-way ANOVA with Tukey's post hoc test).

3.6. Dorsomorphin reverses the protection of ANKRD1 knockdown against DOX-induced cardiomyocyte damage

In vitro experiments using the AMPK inhibitor dorsomorphin were performed. Western blot results showed that AMPK/AKT/mTOR in cells stably knocking down ANKRD1 was inhibited upon dorsomorphin treatment (p-AMPK/AMPK: $p < 0.001$; p-AKT/AKT: $p < 0.001$; p-mTOR/mTOR: $p < 0.05$ vs. shANKRD1 + DOX group) (Fig. 7A; one-way ANOVA with Tukey's post hoc test). Dorsomorphin reversed the promotion of cell viability ($p < 0.01$) and inhibition of LDH release ($p < 0.05$) by ANKRD1 knockdown (Fig. 7B, C; one-way ANOVA with Tukey's post hoc test). Furthermore, dorsomorphin counteracted the increase in mtDNA copy number ($p < 0.001$) and ATP production ($p < 0.05$) by knocking down ANKRD1 (Fig. 7D, E; one-way ANOVA with Tukey's post hoc test), and prevented MMP depolarization ($p < 0.05$, Fig. 7F; one-way ANOVA with Tukey's post hoc test). Additionally, the inhibition of mitochondrial ROS ($p < 0.05$) and intracellular ROS ($p < 0.01$) levels by ANKRD1 knockdown could be partially counteracted by dorsomorphin (Fig. 7G, H; one-way ANOVA with Tukey's post hoc test). Dorsomorphin intervened to reverse the inhibition of cellular oxidative stress by ANKRD1 knockdown (all $p < 0.05$ vs. shANKRD1 + DOX, Fig. 7I; one-way ANOVA with Tukey's post hoc test).

4. Discussion

This study detailed the expression pattern and significant role of ANKRD1 in DOX-induced DCM and clarified its main pathological mechanisms. First, an increase in ANKRD1 expression was identified in the myocardial tissues of rats with DOX-induced DCM and DOX-treated rat cardiomyocytes. This is consistent with the experimental results of Shen et al. [34]. As a nuclear transcriptional cofactor that negatively regulates cardiac gene expression, ANKRD1 overexpression in cardiac tissues by recombinant adenoviruses deteriorates contractile function [35]. ANKRD1 overexpression in transverse aortic constriction mice significantly aggravates cardiac hypertrophy, whereas ANKRD1 downregulation inhibits this condition [36]. How-

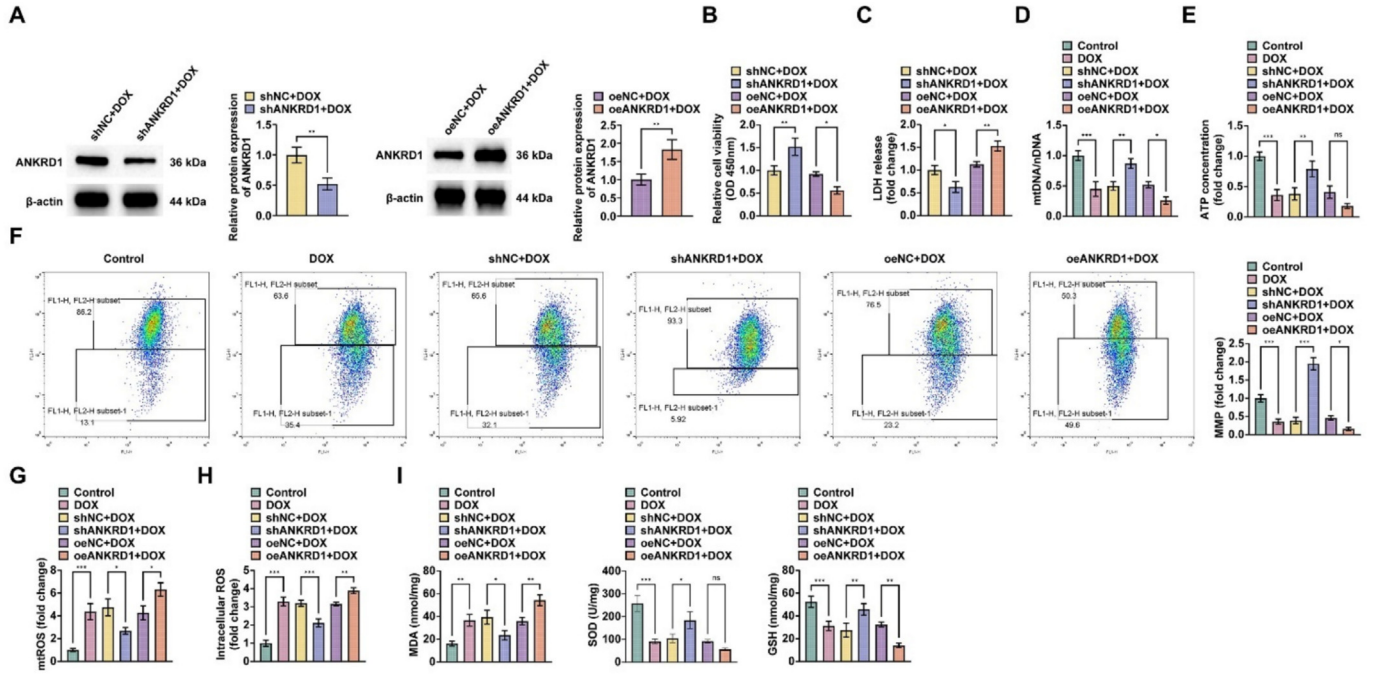

Fig. 5. ANKRD1 knockdown attenuates DOX-induced cardiomyocyte injury, mitochondrial dysfunction and oxidative stress *in vitro*. (A) Western blot detection of protein expression level of cellular ANKRD1; (B) CCK8 assay to detect cell viability; (C) Kit to detect cellular LDH release; (D) RT-qPCR to detect tDNA copy number in cells; (E) Kit to detect ATP content in cells; (F) JC-1 and flow cytometry to detect cellular MMP; (G) MitoSOX and flow cytometry to detect cellular mitochondrial ROS level; (H) DCFH-DA and flow cytometry to detect intracellular ROS level; (I) Kits to detect cellular MDA, SOD, and GSH level. n = 3 biological replicates per group, * $p < 0.05$, ** $p < 0.01$, *** $p < 0.001$, NS: not significant. One-way ANOVA followed by Tukey's post hoc test was used in (B-I), *t* test was used in (A).

ever, the functional characterization of ANKRD1 in DOX-induced DCM has not been fully elucidated. Our data suggested that ANKRD1 knockdown ameliorated cardiac dysfunction and myocardial injury in DOX-induced DCM rats, while increasing ANKRD1 levels worsened these conditions. Nonetheless, previous research on ANKRD1 in cardiac diseases has produced conflicting findings. For example, increasing ANKRD1 expression might reduce myocardial hypertrophy in mice by influencing the extracellular signal-regulated kinase and transforming growth factor-beta pathways [37]. Xie et al. [38] suggested that the conflicting findings on the functional characterization of ANKRD1 in cardiac disorders may be due to the dual function of cytoplasmic and cytosolic ANKRD1, where cytoplasmic ANKRD1 can protect against pressure overload-induced cardiac remodeling, whereas cytosolic ANKRD1 worsens this cardiac remodeling by inducing pathological myosin heavy chain gene 7 activation. Therefore, continued research is essential to further improve our understanding of the link between ANKRD1 and DCM pathophysiology.

Mitochondrial dysfunction and oxidative stress are closely associated with DOX cardiotoxicity [39,40,41]. Mitochondrial dysfunction and OXPHOS abnormalities can lead to an overproduction of ROS, an increase in mitochondrial oxidative stress, and a loss of MMP, which affects the electron transport chain process, hinders ATP synthesis, induces cell death, and ultimately leads to cardiac injury [42]. ANKRD1 overexpression in angiotensin II-stimulated neonatal rat cardiomyocytes enhances mitochondrial permeability and apoptosis, reducing cell viability, whereas ANKRD1 knockdown has the reverse impact [34]. The research similarly indicated that knocking down ANKRD1 mitigated mitochondrial dysfunction and oxidative stress caused by DOX in the myocardial tissues of DCM rats, whereas overexpressing ANKRD1 had the contrary effect. Also, *in vitro*, ANKRD1 knockdown attenuated DOX-induced cardiomyocyte injury, mitochondrial dysfunction and oxidative stress. These findings suggest that the protective effect of targeted ANKRD1 knockdown against DOX cardiotoxicity may be related to the inhibition of mitochondrial dysfunction and oxidative stress.

In eukaryotic cells, AMPK is a major sensor of cellular energy and a key responder to energy homeostasis, trophic homeostasis, and stress responses. AMPK abnormalities are involved in myocardial hypertrophy, inflammatory responses, and myocardial fibrosis by affecting cellular metabolism in cardiac disease pathogenesis. Mitochondrial ROS are physiological activators of AMPK, which mitigates impaired redox homeostasis by enhancing oxidant bioavailability [43,44]. Through the phosphorylation of target proteins, AKT manages cell growth and survival, exerting antiapoptotic effects across several downstream pathways. As a downstream effector of AKT, mTOR is involved in cellular nutrient metabolism and senescence. Activation of AMPK signaling inhibits the AKT/mTOR pathway [45]. It has been recorded that targeting the AMPK/AKT/mTOR pathway alleviates H2O2-induced oxidative damage in cardiomyocytes [46]. Inhibition of AMPK activity by DOX induces DCM by downregulating autophagy to accomplish apoptosis. AMPK activators attenuate DOX-induced DCM, and *in vitro* DOX causes intracellular ROS accumulation in cardiomyocytes, induces mitochondrial damage, leads to an imbalance in intracellular energy metabolism, and triggers apoptosis [33]. Our study further supported the involvement of the AMPK/AKT/mTOR pathway in DOX-induced DCM pathogenesis. As suggested, DOX inhibited p-AMPK, whereas it promoted p-AKT and p-mTOR levels. More interestingly, ANKRD1 knockdown reversed the inhibition of AMPK/AKT/mTOR pathway by DOX, whereas ANKRD1 overexpression showed the opposite effect. Moreover, AMPK inhibitors reversed the protection of ANKRD1 knockdown against DOX-induced cardiomyocyte injury, suggesting that ANKRD1 knockdown activates the AMPK/AKT/mTOR cascade, which attenuates DOX-induced cardiomyocyte cytotoxicity, mitochondrial dysfunc-

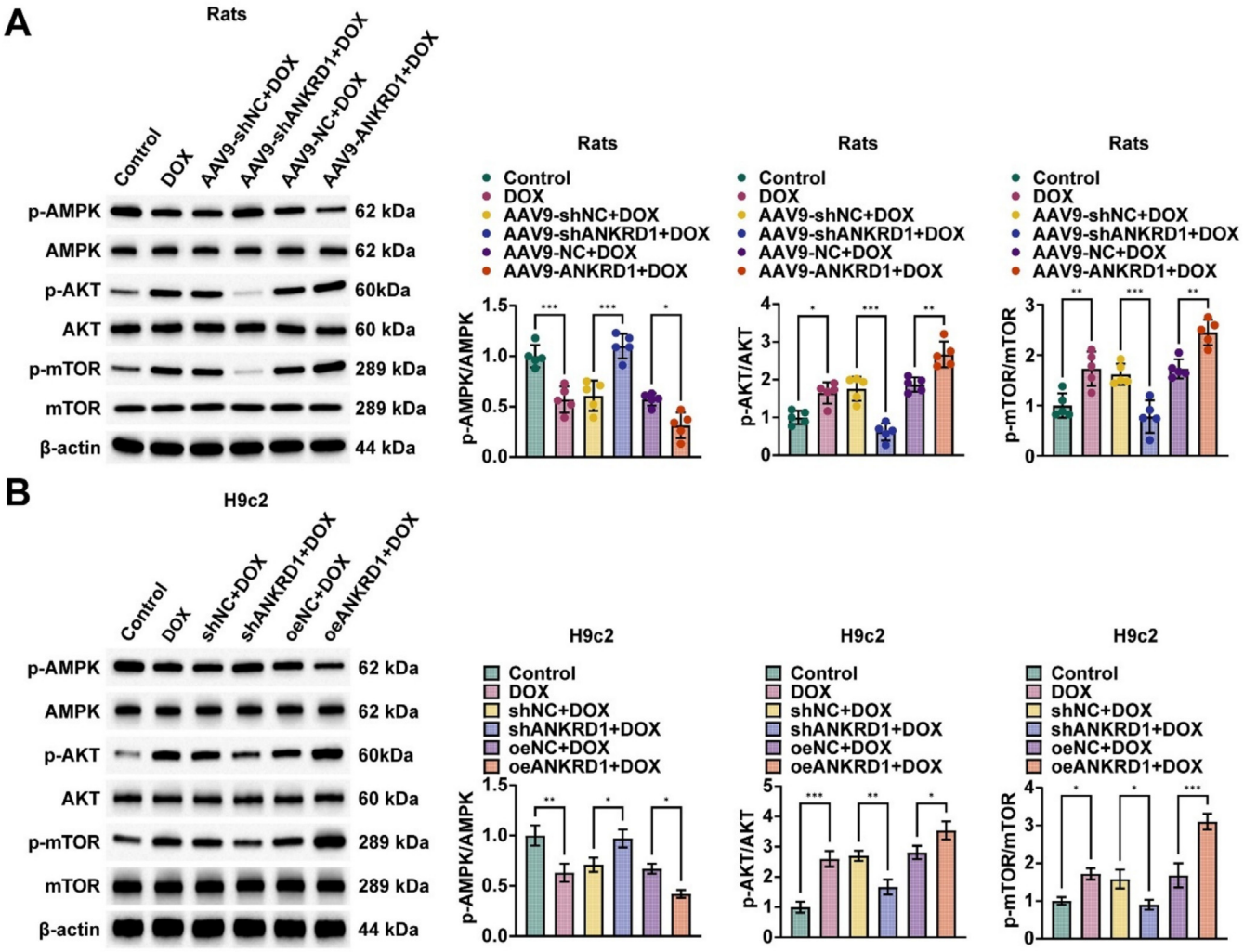

Fig. 6. AMPK/AKT/mTOR pathway is involved in DCM and regulated by ANKRD1. (A) Western blot detection of the expression level of AMPK/AKT/mTOR pathway-related proteins in rat myocardial tissue (n = 5 rats per group); (B) Western blot detection of the expression level of cellular AMPK/AKT/mTOR pathway-related proteins (n = 3 biological replicates per group). * $p < 0.05$, ** $p < 0.01$, *** $p < 0.001$, NS: not significant. All statistical analyses were performed by one-way ANOVA followed by Tukey's post hoc test.

tion, and oxidative stress. These results provide the first mechanistic evidence positioning ANKRD1 as a central mediator of mitochondrial dysfunction and oxidative stress in DOX-induced cardiomyopathy via the AMPK/AKT/mTOR axis.

This study has several limitations. First, while findings from animal and cellular experiments suggest ANKRD1′s potential as an early cardiotoxicity biomarker, clinical translation requires validation in human specimens or patient cohorts. Second, although results demonstrate therapeutic promise, optimal AAV9 dosing parameters and treatment timelines for ANKRD1 modulation in DCM remain unestablished. Future investigations should explore ANKRD1-targeted strategies spanning gene therapies to small-molecule inhibitors. Third, while our DOX-induced models effectively recapitulate key DCM features, they may not fully capture disease complexity. The absence of time-course analyses limits observation of transitional pathophysiology and dose–response dynamics; subsequent studies should incorporate longitudinal assessments to delineate disease progression mechanisms. Finally, due to resource constraints, rescue experiments validating the AMPK/AKT/mTOR pathway were conducted only *in vitro*. *In vivo* verification in the future would strengthen our mechanistic conclusions.

5. Conclusions

Collectively, our study establishes ANKRD1 as a critical regulator of DOX-induced cardiotoxicity. It modulates mitochondrial dysfunction and oxidative stress via the AMPK/AKT/mTOR signaling pathway, as validated by integrated molecular and functional analyses that underscore its therapeutic potential. These findings position ANKRD1 as a promising target for clinical intervention, with translational implications extending from cardiac-specific AAV9-based gene therapies to the development of novel small-molecule inhibitors tailored for precise cardiomyocyte targeting.

CRediT authorship contribution statement

Jia Yuan: Writing – original draft, Visualization, Validation, Software, Resources, Methodology, Conceptualization. **Yu Zhou:** Writing – original draft, Visualization, Validation, Software, Methodology, Data curation, Conceptualization. **GuoHua Wei:** Software, Methodology, Investigation, Formal analysis, Data curation. **Tao Qi:** Visualization, Validation, Investigation, Formal analysis. **HaoLiang Sun:** Writing – review & editing, Supervision, Resources, Project administration, Formal analysis. **Jian Shen:**

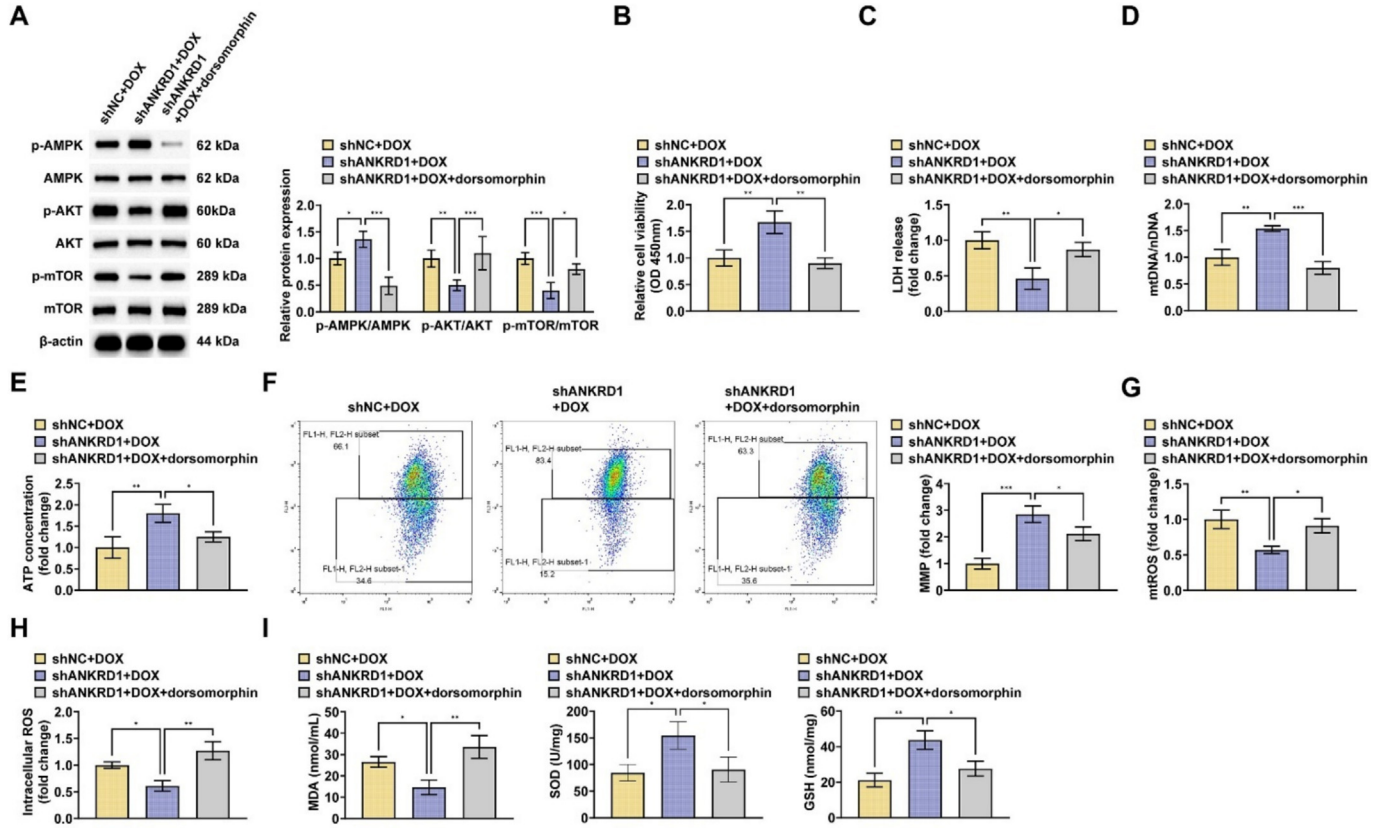

Fig. 7. Dorsomorphin reverses ANKRD1 knockdown and protects against DOX-induced cardiomyocyte injury. (A) Western blot to detect cellular AMPK/AKT/mTOR pathway-related protein expression levels; (B) CCK8 to detect cell viability; (C) Kit to detect cellular LDH release levels; (D) RT-qPCR to detect cellular copy number of mtDNA: (E) Kit to detect cellular ATP content; (F) JC-1 and flow cytometry detection of cellular MMP; (G) MitoSOX and flow cytometry to detect cellular mitochondrial ROS levels; (H) DCFH-DA and flow cytometry to detect intracellular ROS levels; (I) Kits to detect cellular MDA, SOD, and GSH levels. n = 3 biological replicates per group, * $p < 0.05$, ** $p < 0.01$, *** $p < 0.001$, NS: not significant. One-way ANOVA followed by Tukey's post hoc test was used in (B-I), two-way ANOVA followed by Tukey's post hoc test was used in (A).

Writing – review & editing, Supervision, Project administration, Funding acquisition, Data curation.

Ethical approval (animals)

All animal experiments were complied with the ARRIVE guidelines and performed in accordance with the National Institutes of Health Guide for the Care and Use of Laboratory Animals. The experiments were approved by the Institutional Animal Care and Use Committee of Jiangsu Province Hospital (No. 2021-SRFA-023).

Financial support

Jiangsu Province Capability Improvement Project through Science, Technology, and Education (No. ZDXK202230).

Declaration of competing interest

The authors declare that they have no known competing financial interests or personal relationships that could have appeared to influence the work reported in this paper.

Supplementary material

https://doi.org/10.1016/j.ejbt.2025.08.002.

Data availability

Data will be made available on request.

References

[1] Weintraub RG, Semsarian C, Macdonald P. Dilated cardiomyopathy. Lancet 2017;390(10092):400–14. https://doi.org/10.1016/s0140-6736(16)31713-5. PMid: 28190577.
[2] Heymans S, Lakdawala NK, Tschöpe C, et al. Dilated cardiomyopathy: Causes, mechanisms, and current and future treatment approaches. Lancet 2023;402 (10406):998–1011. https://doi.org/10.1016/s0140-6736(23)01241-2. PMid: 37716772.
[3] Reichart D, Magnussen C, Zeller T, et al. Dilated cardiomyopathy: From epidemiologic to genetic phenotypes. A translational review of current literature. J Intern Med 2019;286(4):362–72. https://doi.org/10.1111/joim.12944. PMid: 31132311.
[4] Orphanou N, Papatheodorou E, Anastasakis A. Dilated cardiomyopathy in the era of precision medicine: Latest concepts and developments. Heart Fail Rev 2022;27(4):1173–91. https://doi.org/10.1007/s10741-021-10139-0. PMid: 34263412.
[5] Harding D, Chong MHA, Lahoti N, et al. Dilated cardiomyopathy and chronic cardiac inflammation: Pathogenesis, diagnosis and therapy. J Intern Med 2023;293(1):23–47. https://doi.org/10.1111/joim.13556. PMid: 36030368.
[6] Kankeu C, Clarke K, Passante E, et al. Doxorubicin-induced chronic dilated cardiomyopathy-the apoptosis hypothesis revisited. J Mol Med 2017;95 (3):239–48. https://doi.org/10.1007/s00109-016-1494-0. PMid: 27933370.
[7] Sun M, Zhang X, Tan B, et al. Potential role of endoplasmic reticulum stress in doxorubicin-induced cardiotoxicity-an update. Front Pharmacol 2024;15:1415108. https://doi.org/10.3389/fphar.2024.1415108. PMid: 39188945.

[8] Zhang P, Lu H, Wu Y, et al. COX5A alleviates doxorubicin-induced cardiotoxicity by suppressing oxidative stress, mitochondrial dysfunction and cardiomyocyte apoptosis. Int J Mol Sci 2023;24(12):10400. https://doi.org/10.3390/ijms241210400. PMid: 37373547.
[9] Da Dalt L, Cabodevilla AG, Goldberg IJ, et al. Cardiac lipid metabolism, mitochondrial function, and heart failure. Cardiovasc Res 2023;119(10):1905–14. https://doi.org/10.1093/cvr/cvad100. PMid: 37392421.
[10] Chistiakov DA, Shkurat TP, Melnichenko AA, et al. The role of mitochondrial dysfunction in cardiovascular disease: A brief review. Ann Med 2018;50(2):121–7. https://doi.org/10.1080/07853890.2017.1417631. PMid: 29237304.
[11] Huang Y, Li W, Sun H, et al. Mitochondrial transfer in the progression and treatment of cardiac disease. Life Sci 2024;358:123119. https://doi.org/10.1016/j.lfs.2024.123119. PMid: 39395616.
[12] Sharma S, Bhattarai S, Ara H, et al. SOD2 deficiency in cardiomyocytes defines defective mitochondrial bioenergetics as a cause of lethal dilated cardiomyopathy. Redox Biol 2020;37:101740. https://doi.org/10.1016/j.redox.2020.101740. PMid: 33049519.
[13] Li E, Li X, Huang J, et al. BMAL1 regulates mitochondrial fission and mitophagy through mitochondrial protein BNIP3 and is critical in the development of dilated cardiomyopathy. Protein Cell 2020;11(9):661–79. https://doi.org/10.1007/s13238-020-00713-x. PMid: 32277346.
[14] Enomoto H, Mittal N, Inomata T, et al. Dilated cardiomyopathy-linked heat shock protein family D member 1 mutations cause up-regulation of reactive oxygen species and autophagy through mitochondrial dysfunction. Cardiovasc Res 2021;117(4):1118–31. https://doi.org/10.1093/cvr/cvaa158. PMid: 32520982.
[15] Du H, Zhao Y, Wen J, et al. LncRNA DCRT protects against dilated cardiomyopathy by preventing NDUFS2 alternative splicing by binding to PTBP1. Circulation 2024;150(13):1030–49. https://doi.org/10.1161/circulationaha.123.067861. PMid: 38841852.
[16] Peoples JN, Saraf A, Ghazal N, et al. Mitochondrial dysfunction and oxidative stress in heart disease. Exp Mol Med 2019;51(12):1–13. https://doi.org/10.1038/s12276-019-0355-7. PMid: 31857574.
[17] Ramaccini D, Montoya-Uribe V, Aan FJ, et al. Mitochondrial function and dysfunction in dilated cardiomyopathy. Front Cell Dev Biol 2020;8:624216. https://doi.org/10.3389/fcell.2020.624216. PMid: 33511136.
[18] Xie S, Sun Y, Zhao X, et al. An update of the molecular mechanisms underlying anthracycline induced cardiotoxicity. Front Pharmacol 2024;15:1406247. https://doi.org/10.3389/fphar.2024.1406247. PMid: 38989148.
[19] Han Q, Shi J, Yu Y, et al. Calycosin alleviates ferroptosis and attenuates doxorubicin-induced myocardial injury via the Nrf2/SLC7A11/GPX4 signaling pathway. Front Pharmacol 2024;15:1497733. https://doi.org/10.3389/fphar.2024.1497733. PMid: 39600362.
[20] Ye J, Huang Y, Que B, et al. Interleukin-12p35 knock out aggravates doxorubicin-induced cardiac injury and dysfunction by aggravating the inflammatory response, oxidative stress, apoptosis and autophagy in mice. EBioMedicine 2018;35:29–39. https://doi.org/10.1016/j.ebiom.2018.06.009. PMid: 30228093.
[21] Wang Z, Wang M, Liu J, et al. Inhibition of TRPA1 attenuates doxorubicin-induced acute cardiotoxicity by suppressing oxidative stress, the inflammatory response, and endoplasmic reticulum stress. Oxid Med Cell Longev 2018;2018(1):5179468. https://doi.org/10.1155/2018/5179468. PMid: 29682158.
[22] Moulik M, Vatta M, Witt SH, et al. *ANKRD1*, the gene encoding cardiac ankyrin repeat protein, is a novel dilated cardiomyopathy gene. J Am Coll Cardiol 2009;54(4):325–33. https://doi.org/10.1016/j.jacc.2009.02.076. PMid: 19608030.
[23] Mastrototaro G, Carullo P, Zhang J, et al. Ablation of palladin in adult heart causes dilated cardiomyopathy associated with intercalated disc abnormalities. Elife 2023;12:e78629. https://doi.org/10.7554/eLife.78629. PMid: 36927816.
[24] Bogomolovas J, Brohm K, Čelutkienė J, et al. Induction of Ankrd1 in dilated cardiomyopathy correlates with the heart failure progression. Biomed Res Int 2015;2015(1):273936. https://doi.org/10.1155/2015/273936. PMid: 25961010.
[25] Ma X, Mo C, Huang L, et al. Robust rank aggregation and least absolute shrinkage and selection operator analysis of novel gene signatures in dilated cardiomyopathy. Front Cardiovasc Med 2021;8:747803. https://doi.org/10.3389/fcvm.2021.747803. PMid: 34970603.
[26] Piroddi N, Pesce P, Scellini B, et al. Myocardial overexpression of ANKRD1 causes sinus venosus defects and progressive diastolic dysfunction. Cardiovasc Res 2020;116(8):1458–72. https://doi.org/10.1093/cvr/cvz291. PMid: 31688894.
[27] Murphy NP, Lubbers ER, Mohler PJ. Advancing our understanding of AnkRD1 in cardiac development and disease. Cardiovasc Res 2020;116(8):1402–4. https://doi.org/10.1093/cvr/cvaa063. PMid: 32186710.
[28] Rinkūnaitė I, Šimoliūnas E, Alksnė M, et al. Genetic ablation of Ankrd1 mitigates cardiac damage during experimental autoimmune myocarditis in mice. Biomolecules 2022;12(12):1898. https://doi.org/10.3390/biom12121898. PMid: 36551326.
[29] Shen LJ, Lu S, Zhou YH, et al. Developing a rat model of dilated cardiomyopathy with improved survival. J Zhejiang Univ Sci B 2016;17(12):975–83. https://doi.org/10.1631/jzus.B1600257. PMid: 27921402.
[30] Pang XF, Lin X, Du JJ, et al. LTBP2 knockdown by siRNA reverses myocardial oxidative stress injury, fibrosis and remodelling during dilated cardiomyopathy. Acta Physiol (Oxf) 2020;228(3):e13377. https://doi.org/10.1111/apha.13377. PMid: 31512380.
[31] Zhu M, Chen Y, Cheng L, et al. Calsyntenin-1 promotes doxorubicin-induced dilated cardiomyopathy in rats. Cardiovasc Drugs Ther 2024;38(2):237–52. https://doi.org/10.1007/s10557-022-07389-x. PMid: 36350487.
[32] Zhang L, Zhang Y, Chen D, et al. Value of label-free ubiquitin-proteomic analysis on defining the protective mechanism of valsartan against doxorubicin-induced heart failure. Curr Cancer Drug Targets 2025;25(7):795–805. https://doi.org/10.2174/0115680096341637241231111922. PMid: 39817389.
[33] Zhang S, Wei X, Zhang H, et al. Doxorubicin downregulates autophagy to promote apoptosis-induced dilated cardiomyopathy via regulating the AMPK/mTOR pathway. Biomed Pharmacother 2023;162:114691. https://doi.org/10.1016/j.biopha.2023.114691. PMid: 37060659.
[34] Shen L, Chen C, Wei X, et al. Overexpression of ankyrin repeat domain 1 enhances cardiomyocyte apoptosis by promoting p53 activation and mitochondrial dysfunction in rodents. Clin Sci (Lond) 2015;128(10):665–78. https://doi.org/10.1042/cs20140586. PMid: 25511237.
[35] Zolk O, Marx M, Jäckel E, et al. β-adrenergic stimulation induces cardiac ankyrin repeat protein expression: Involvement of protein kinase A and calmodulin-dependent kinase. Cardiovasc Res 2003;59(3):563–72. https://doi.org/10.1016/s0008-6363(03)00476-0. PMid: 14499857.
[36] Chen C, Shen L, Cao S, et al. Cytosolic CARP promotes angiotensin II- or pressure overload-induced cardiomyocyte hypertrophy through calcineurin accumulation. PLoS One 2014;9(8):e104040. https://doi.org/10.1371/journal.pone.0104040. PMid: 25089522.
[37] Song Y, Xu J, Li Y, et al. Cardiac ankyrin repeat protein attenuates cardiac hypertrophy by inhibition of ERK1/2 and TGF-β signaling pathways. PLoS One 2012;7(12):e50436. https://doi.org/10.1371/journal.pone.0050436. PMid: 23227174.
[38] Xie R, Yuan S, Hu G, et al. Nuclear AGO2 promotes myocardial remodeling by activating ANKRD1 transcription in failing hearts. Mol Ther 2024;32(5):1578–94. https://doi.org/10.1016/j.ymthe.2024.03.018. PMid: 38475992.
[39] Tomczyk MM, Cheung KG, Xiang B, et al. Mitochondrial Sirtuin-3 (SIRT3) prevents doxorubicin-induced dilated cardiomyopathy by modulating protein acetylation and oxidative stress. Circ Heart Fail 2022;15(5):e008547. https://doi.org/10.1161/circheartfailure.121.008547. PMid: 35418250.
[40] Shipra MK, Tembhre MP, Hote, et al. PGC-1α agonist rescues doxorubicin-induced cardiomyopathy by mitigating the oxidative stress and necroptosis. Antioxidants 2023;12(9):1720. https://doi.org/10.3390/antiox12091720. PMid: 37760023.
[41] Zhao J, Yang T, Yi J, et al. AP39 through AMPK-ULK1-FUNDC1 pathway regulates mitophagy, inhibits pyroptosis, and improves doxorubicin-induced myocardial fibrosis. iScience 2024;27(4):109321. https://doi.org/10.1016/j.isci.2024.109321. PMid: 38558936.
[42] Murphy E, Liu JC. Mitochondrial calcium and reactive oxygen species in cardiovascular disease. Cardiovasc Res 2023;119(5):1105–16. https://doi.org/10.1093/cvr/cvac134. PMid: 35986915.
[43] Rabinovitch RC, Samborska B, Faubert B, et al. AMPK maintains cellular metabolic homeostasis through regulation of mitochondrial reactive oxygen species. Cell Rep 2017;21(1):1–9. https://doi.org/10.1016/j.celrep.2017.09.026. PMid: 28978464.
[44] Gao Y, Zhao D, Xie WZ, et al. Rap1GAP mediates angiotensin II-induced cardiomyocyte hypertrophy by inhibiting autophagy and increasing oxidative stress. Oxid Med Cell Longev 2021;2021(1):7848027. https://doi.org/10.1155/2021/7848027. PMid: 33936386.
[45] Lin SC, Hardie DG. AMPK: Sensing glucose as well as cellular energy status. Cell Metab 2018;27(2):299–313. https://doi.org/10.1016/j.cmet.2017.10.009. PMid: 29153408.
[46] Wang Y, Sun D, Chen Y, et al. Alkaloids of *Delphinium grandiflorum* and their implication to H_2O_2-induced cardiomyocytes injury. Bioorg Med Chem 2021;37:116113. https://doi.org/10.1016/j.bmc.2021.116113. PMid: 33744825.